# Effort generation capabilites mapping for personalized robotic assistance of the elbow

Mael Gallois, Maxime Manzano, Sylvain Guégan, Nicolas Vignais, Marie Babel, Charles Pontonnier

# Effort generation capabilites mapping for personalized robotic assistance of the elbow

Maël Gallois[1], Maxime Manzano[2], Sylvain Guegan [3], Nicolas Vignais [4], Marie Babel [2] and Charles Pontonnier[1]

***Abstract*— This study explores the use of a robotic aid to improve the mobility of people with neuromuscular or neurodegenerative disorders, who have reduced motor skills. It aims to compare the use of either a musculoskeletal model or a torque-angle joint model in a shared control framework of an upper limb exoskeleton in order to assists elbow flexion/extension movements. The method consists of measuring the effort-generating capacities of the elbow using an isokinetic ergometer. Data were then used to calibrate the two models. Both were integrated into an exoskeleton control law to estimate online user isometric capacities during a mass-holding task performed in various positions. Four experimental conditions were compared: without exoskeleton, with exoskeleton without assistance, with assistance computed from the quadratic model and from the musculoskeletal model. In order to test the method against individual variability, the study was conducted with nine participants. The results show a decrease in muscular activity for the biceps in both assistance conditions. In extrapolating effort-generating capacities outside the ergometer's measured range, the musculoskeletal model is more robust than the torque-angle joint model. Its estimations are more consistent with the literature, while torque-angle joint model errors induces unintended triceps activation. In conclusion, this study highlights the potential of combining a musculoskeletal model with shared control for assisting elbow.**

## I. INTRODUCTION

Upper limb assistance is essential for individuals with neuromuscular or neurodegenerative disorders, which hinder their ability to perform daily tasks and reduce their autonomy. Robotic assistance can then help restore independence by partially or fully supporting the user's actions.

Currently, shared control is a widely used approach in the field of robotic assistance. This collaborative method involves to share the control responsibility between the human and the robot during task execution. An effective implementation requires accurately interpreting the user's intentions and generating commands tailored to the task and the user's specific needs. Admittance control is a common strategy of shared control for assitive robotic: it adjusts the robot position or velocity in response to the measured interaction forces or torques [1].

However, designing efficient shared control systems requires to adapt the provided assistance to the user capabilities, and can be challenging in particular for users that face multiple mobility impairments. To alleviate this issue, one solution is to accurately estimate the effort-generating capacity of users and take this information into account in the assistive control, thus enhancing user experience [2].

Incorporating user capability estimates into exoskeleton control effectively adapts assistance, as it has been shown in a walking-assistance systems [3]. A similar strategy could benefit upper-limb assistance. In this case, for instance, effort capability estimators have been used in minimal assist-as-needed (mAAN) controllers for static poses [4]. However, the personalization of these estimations in the field of upper limb assistive robotics remains unexplored in the literature.

Nonetheless, works have already been made to represent effort generation capabilities. For example, joint torque generation capabilities have been represented as joint torque-angle relationships [5], specifically as a quadratic function in the case of the elbow [6]. Alternatively, such works have been used to calibrate musculoskeletal models with individualized parameters from experimental measurements [7], [8]. These models could then be used to estimate effort-generating capacities of the user [9]. In turn, these biomechanical representations can be used to personalize robotic assistance.

Here, we aim to integrate a personalized estimator of the user's effort generation capabilities into the shared control of an upper-limb exoskeleton. The objective of this study is then to compare two force capabilities representations, i.e. torque-angle model and musculoskeletal model. For instance, we focused in the context of elbow assistance. In Section II, we present two estimators based on experimental measurements. The first is a quadratic torque-angle model (TAM). The second is a personnalized musculoskeletal model (MSM) based on the Saul et al. upper limb model [10]. Then, a control law derived from these two effort generation capabilities representations is introduced and an experimental evaluation is proposed. Section III presents and discusses the evaluation results. Finally, Section IV provides a conclusion.

## II. MATERIALS AND METHODS

This section presents two methods of effort generation capabilities estimators. Subsequently, an assistive control law utilising a effort estimator is described, as well as a proposed experimental protocol.

### A. Torque-angle joint model (TAM)

The objective is to obtain the torque-angle relationship of the elbow. This requires to measure the maximum isometric

[1]Univ Rennes, Inria, CNRS, IRISA - UMR 6074, F-35000 Rennes, France, mael.gallois@inria.fr

[2]Univ Rennes, INSA Rennes, Inria, CNRS, IRISA - UMR 6074, F-35000 Rennes, France

[3]Univ Rennes, INSA Rennes, LGCGM, F-35000 Rennes, France

[4]M2S Laboratory, Rennes 2 Université, École Normale Supérieure de Rennes, F-35000 Rennes, France

torque $\tau_{isom}$ in flexion ($\tau_{isom} > 0$) and extension ($\tau_{isom} < 0$) over the joint amplitude. Directly measuring isometric torque for each position in the workspace is time-intensive and may cause significant fatigue for the participant. To optimize the process and limit fatigue, we proposed to conduct isokinetic tests, i.e. at a constant speed. However, as muscles capacities are non-linearly coupled with speed values, these tests inherently alter the elbow torque values. To address this issue, we performed tests in two distinct configurations for each direction of efforts (flexion and extension), namely concentric (effort in the direction of movement) and eccentric (effort opposing the movement). These measurements $\tau_{mes}$ are obtained using an isokinetic ergometer (see Figure 1), a device designed for rehabilitation that measures joint capacities using a torque sensor aligned with the rotational axis of the participant's joint. The ergometer imposed a constant speed of 30 degrees per second, which was considered to be sufficiently low to ensure a near-linear relationship between torque and speed variation [5]. This linearity allowed us to approximate the isometric torque curve by averaging the results of both concentric and eccentric tests. Each of the four configurations was repeated three times, and for each elbow angle, we retained the maximum value measured.

Fig. 1. The isokinetic ergometer used for joint torque measurements (ConTrex, Medimex).

The experiment was validated by the Operational Committee for the Evaluation of Legal and Ethical Risks (COERLE) of the Inria institute. Nine participants took part in the study (height in cm: 175.3 ± 5.4, weight in kg: 70.3 ± 9.54, age in years : 25.8 ± 8.6). The joint range of elbow motion varied between participants, with a mean range of 60.2±3.2 to 126.8±5.8 degrees. Using the collected data, we fit two quadratic TAMs to the experimental isometric torque curves for both flexion and extension

### *B. Personnalized musculoskeletal model (MSM)*

The MSM is composed of two layers. The first layer consists of an osteoarticular model describing geometrical and inertial properties of the upper limb. It is represented as a two-dimensional system composed of three rigid bodies: the trunk (considered as a fixed reference frame), the arm, and the forearm/hand. These rigid bodies are connected by two revolute joints, simulating the flexion/extension motions of the shoulder and elbow. The joint angles are denoted as $q_1$ (shoulder) and $q_2$ (elbow).

The second layer of the MSM is the actuation model, consisting in muscles lines attached to the osteoarticular model. The muscles behavior is based on the Hill-Zajac model [11], ans the model incorporates $N_m = 12$ muscles. Their insertion points and physiological properties following the description made by Saul et al. [10]. Each muscle line $j \in \{1;N_m\}$ is composed of three elements:

- a passive element modeling the tendon with a length of $l_{sj}$, assumed to be non-deformable to reduce computational complexity;
- an active element of lenght $l_{mj}$ represents the contractile active force generated by the muscle $F_{aj}$;
- parallel to the active element, a nonlinear spring models the passive properties of the muscle fiber producing $F_{pj}$.

The total muscle line $j$ force is therefore $F_{aj} + F_{pj}$, and its total length is $l_{mj} + l_{sj}$.

Muscle lengths vary according to the position of the osteoarticular model. The force-length characteristic is defined by its maximum voluntary force $F_{0j}$, and the muscle length at which it can be produce, i.e. the optimal muscle fiber length $l_{0j}$. We define $\tilde{l}_{mj} = \frac{l_{mj}}{l_{0j}}$ as the normalized muscle fiber length. As did [12] and [7], we also defined the minimum (resp. maximum) length of the force-length characteristic: $\tilde{l}_{minj}$ (resp. $\tilde{l}_{maxj}$). This two length parameterize the shape of the characteristic without modifying the anatomic values of $l_{0j}$ and $l_{sj}$, so that

$$F_{aj}(\tilde{l}_{mj}) = \begin{cases} F_{0j}\left(\frac{\tilde{l}_{minj}^2(\tilde{l}_{minj}-3)}{(\tilde{l}_{minj}-1)^3} + \frac{6\tilde{l}_{minj}}{(\tilde{l}_{minj}-1)^3}\tilde{l}_{mj} - \frac{3(\tilde{l}_{minj}+1)}{(\tilde{l}_{minj}-1)^3}\tilde{l}_{mj}^2 \right. \\ \qquad \left. + \frac{2}{(\tilde{l}_{minj}-1)^3}\tilde{l}_{mj}^3\right) \qquad \text{if } \tilde{l}_{mj} < 1 \\ F_{0j}\left(\frac{\tilde{l}_{maxj}^2(\tilde{l}_{maxj}-3)}{(\tilde{l}_{maxj}-1)^3} + \frac{6\tilde{l}_{maxj}}{(\tilde{l}_{maxj}-1)^3}\tilde{l}_{mj} - \frac{3(\tilde{l}_{maxj}+1)}{(\tilde{l}_{maxj}-1)^3}\tilde{l}_{mj}^2 \right. \\ \qquad \left. + \frac{2}{(\tilde{l}_{maxj}-1)^3}\tilde{l}_{mj}^3\right) \qquad \text{if } \tilde{l}_{mj} \geq 1 \end{cases} \tag{1}$$

for active forces, and

$$F_{pj}(\tilde{l}_{mj}) = \begin{cases} 0 \qquad \text{if } \tilde{l}_{mj} < 1 \\ F_{0j}\left(\frac{5}{4(\tilde{l}_{maxj}-1)^2} - \frac{5}{2(\tilde{l}_{maxj}-1)^2}\tilde{l}_{mj} + \frac{5}{4(\tilde{l}_{maxj}-1)^2}\tilde{l}_{mj}^2\right) \\ \qquad \text{if } \tilde{l}_{mj} \geq 1 \end{cases} \tag{2}$$

for passive forces. The figure 2 shows the normalized characteristic behavior of this Hill-Zajac model. Then, each muscle $j \in \{1;N_m\}$ exerts a torque around joint $i \in \{1;2\}$ defined as

$$\tau_{i,j}^{model} = \left[F_{aj}(\tilde{l}_{mj}) + F_{pj}(\tilde{l}_{mj})\right]\frac{\partial l_{mj}}{\partial q_i}. \tag{3}$$

In order to personalize this MSM, two successive steps were implemented. First, segment and muscle paths were scaled simultaneously, adjusting muscle length parameters ($l_{0j}$ and $l_{sj}$) to match participant segment sizes (Figure 3). Maximum voluntary forces $F_{0j}$ were then linearly adjusted

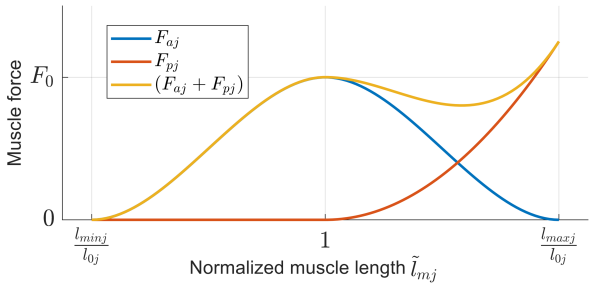


Fig. 2. Normalized force-length characteristic of a muscle line model [7].

based on the initial Saul model's torque maximal capacity and the ergometer's maximal measured torque, ensuring consistency between model geometry and muscle capacities. The scaling used the same measurements as those defining the TAM in II-A.

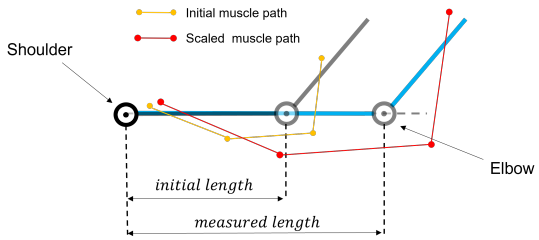


Fig. 3. Schematic diagram of arm scaling and muscle pathway scaling.

The second step consists of calibrating muscle parameters $\tilde{l}_{minj}$ and $\tilde{l}_{maxj}$ using ergometer torque measurements. This involved an optimization process to minimize the difference between the measured torque $\tau_{mes}$ and the MSM estimated muscle torques around the elbow, such that

$$\min_{\mathbf{F_0},\tilde{\mathbf{l}}_{\mathbf{min}},\tilde{\mathbf{l}}_{\mathbf{max}}} \left(\tau_2^{model} - \tau_{mes}\right)^2, \quad \text{with } \tau_2^{model} = \sum_{j=1}^{N_m} \tau_{2,j}^{model}. \quad (4)$$

$\{\mathbf{F_0},\tilde{\mathbf{l}}_{\mathbf{min}},\tilde{\mathbf{l}}_{\mathbf{max}}\} = \{(F_{0j}),(\tilde{l}_{minj}),(\tilde{l}_{maxj})\}_{i=1}^{N_m}$ are the optimisation variables. As they do not have the same same order of magnitude, we successively optimized the length parameters and the force parameters until the problem converged.

### C. Assistance control law

The control scheme employs an admittance filter for torque control. Furthermore, two modes have been implemented: transparent and assisted.

Transparent mode, as defined by W. van Dijk et al. [13], eliminates the interaction forces between the user and the robot, ensuring the robot does not resist against user movements. To do that, two strategies are discussed in the literature [14]. The first aims to compensate the dynamics of the exoskeleton. In this work, only the exoskeleton gravity $\mathbf{G}(\mathbf{q})$ was computed and compensated. The second strategy is to use force measurement to impose a zero interaction force. The control scheme shown in figure 4 was therefore used for this work, where $J$ is the exoskeleton Jacobian. In the case of transparent mode, the reference torque input $\tau^*$ is set to 0.

The assisted mode (with a non zero $\tau^*$) aimed to provide assistance according to the effort required by a task, in order to limit the user's contribution to a predefined percentage of their maximum force. The torque required for the task $\tau_{task}$ was estimated statically with

$$\tau_{task} = g(m_{obj}L_f + m_f L_{fmc}), \quad (5)$$

knowing the mass of the object carried by the user $m_{obj}$ and the mass of his forearm $m_f$. The forearm length $L_f$ was measured at the start of the experiment and the lever arm of the forearm's center of mass $L_{fmc}$ was known from the osteoarticular model. $g$ is the gravity acceleration.

The assistance principle is illustrated in Figure 5 and is obtained by computing

$$\tau^* = \begin{cases} 0 & \text{if } |\tau_{task}| < 0.03 \times |\tau_2^{model}| \\ \tau_{task} - 0.03 \times \tau_2^{model} & \text{otherwise.} \end{cases} \quad (6)$$

This combines the advantages of a transparent mode (preserved user control) and a physical assistance (reduced fatigue). We set this threshold at 3% of the maximum voluntary force $\tau_2^{model}$ estimated by either the TAM or MSM. This threshold is lower than the recommendations of [15], which suggest a maximal value of 10% to avoid fatigue. This value remains then completely adjustable. Effort generation capacities are then estimated in real time using either the TAM or the MSM according to equation (3).

### D. Experimental setup

Nine participants, whose elbow torque generation capabilities were measured (II-A), sat in a stationary power wheelchair on which the exoskeleton is attached. The setup included an optoelectronic motion capture system (Nine Qualisys Miqus) sampled at 100 Hz. Fifteen markers, each with a diameter of 14 mm, were placed on the participant at standardized anatomical landmarks following the guidelines of the International Society of Biomechanics [16]. The exoskeleton is capable of assisting the abduction of the shoulder and the flexion of both the shoulder and the elbow [17]. In the present case study, shoulder movements are locked. Figure 6 illustrates the experimental setup. In addition, electromyographic sensors (EMG) were placed on the following muscles, according to the SENIAM standard [18]: Triceps Long Head, Anterior Deltoid, Posterior Deltoid, Medial Deltoid, Biceps. These sensors operated at 1259Hz. Once installed in the wheelchair, the participant's arm was positioned in the exoskeleton using a 3D-printed support in which the arm rests, and the forearm was positioned using a 3D-printed orthosis. A screen was positioned in front of the participant. This screen displayed feedback on the angular position of the elbow and a target zone. For position feedback, data from the encoder of the exoskeleton were used. The position feedback delay was less than 20ms. The control was fully implemented in a dSPACE system running at 5 kHz. Motion capture and EMGs were not used for control, but only for evaluation.

Participants were asked to perform a task involving moving/holding a cylindrical object with a mass of 1kg. The set

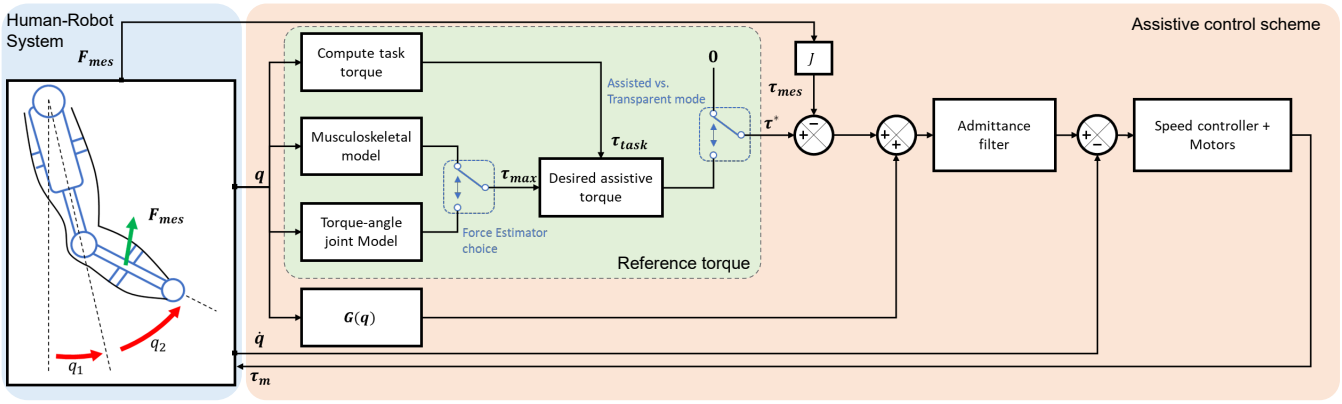


Fig. 4. Architecture of the assistive control. Human-robot interaction force is measured for torque control, and robot gravity is compensated. $J$ is the exoskeleton Jacobian.

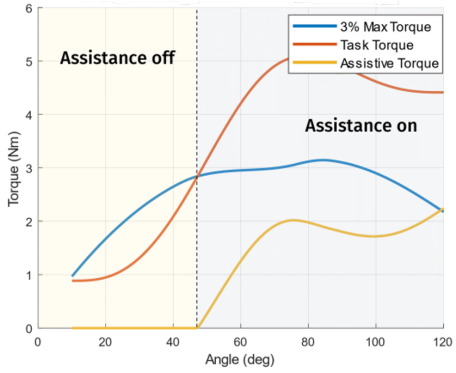


Fig. 5. Principle of the assistance provided by the exoskeleton according to the torque required by the task.

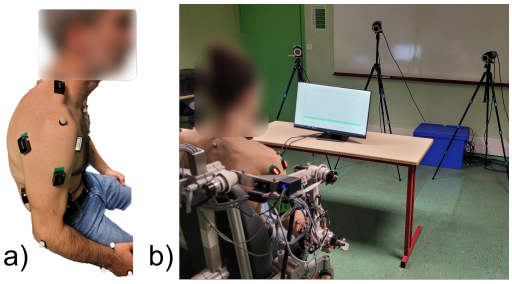


Fig. 6. a) Six EMG on arm and shoulder muscles and markers. b) Experimental setup. The participant is positioned in the exoskeleton, which is mounted on an power wheelchair. A display shows the angle to be reached with feedback on the position in real time.

trajectory comprised five steps of 10 seconds at 20°, 60°, 100°, 60° and 20°. It was performed in 4 configurations:

- No-Exo mode: the participant performs the task without the exoskeleton;
- Transparent mode: the reference torque $\tau^*$ is set to 0;
- Torque-Angle based Control (TAC) mode: the reference torque $\tau^*$ is computed from the TAM;
- Musculoskeletal based Control (MSC) mode: the reference torque $\tau^*$ is computed from the MSM.

### *E. Data processing*

The EMG data were rectified and filtered with a Root Mean Squared (RMS) filter to obtain the signal envelope with a 500ms window. The filter window was deliberately chosen to correspond to slow or static tasks, as recommended in the literature [19]. For each participant and for each EMG sensor, the signal was normalized to the highest value of the envelope recorded during the No-Exo test.

Data from the optoelectronic system were converted into joint angles using the OpenSim software [20]. The osteoarticular model used for this step is the one developed by Seth *et al.* [21]. This kinematic model enables the investigation of potential shoulder translational motion when the subject wears the exoskeleton.

An estimate of the torque provided by the participant was made by taking the difference between the torque of the task $\tau_{task}$ and the measurement of the torque exerted by the exoskeleton. It is given by

$$\tau_p = \tau_{task} - \tau_{mes}. \tag{7}$$

Finally, the data set was temporally normalized over the duration of one repetition of the task. As the timing was imposed, identically lasting 50 seconds.

## III. RESULTS AND DISCUSSIONS

Figure 7 displays the personalized MSM parameters $\{\mathbf{l_s}, \mathbf{l_0}, \mathbf{F_0}\}$ for the elbow muscles. The parameters' values remained consistent with to the parameters defined in the Saul model [10] and with values reported in the literature. However, the triceps muscles appeared to be more powerful (bigger $F_{0j}$) in our study compared to those described in the Saul model. This inconsistency was likely due to the testing position in the ergometer, in which participants were able to lean against the machine, artificially increasing the measured torque values. Figure 8 illustrates the mean estimated torques for the MSMs and TAMs. The torque-angle relationships generated by the two estimators were closely aligned within the range of experimental measurements. However, outside this range of measures, the estimations given by the two models divergeds. Near the lower limit of elbow joint motion, the TAM produced inconsistent effort-generating capacities, even changing sign for some participants. In contrast, the MSM exhibited a curve shape that is more closely aligned with the original Saul model that appears to be consistent with the actual capabilities of the elbow [5].

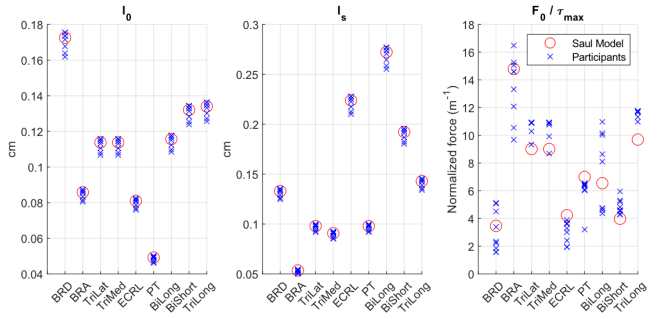


Fig. 7. Muscle characteristics of customized MSMs for muscles acting on the elbow. For each participant, each $F_0$ parameter is normalized to the maximum torque $\tau max$ that a participant can produce. Muscles are Brachioradialis (BRD), Brachialis (BRA), Triceps Lateral head (TriLat), Triceps Medial head(TriMed), Extensor Carpi Radialis Longus (ECRL), Pronator Teres (PT), Biceps Long head (BiLong), Biceps Short head (BiShort) and Triceps Long head(TriLong).

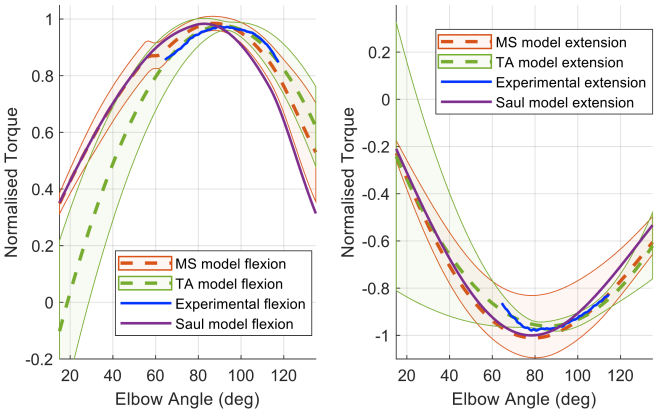


Fig. 8. Torque-angle relationships in flexion (left) and extension (right). Torque is normalized by its maximum value, then averaged over all participants. Standards deviations of the MSM and TAM are plotted as a zone.

Figure 9 illustrates the estimated torque results for the participants. In both assisted configurations (TAC and MSC), as expected, the average torque supplied by the participants was lower than the one provided in the transparent configuration. During static phases, the 3% user effort limit was better maintained compared to the dynamic phases. Indeed one of the main challenges of admittance control is improving reactivity while ensuring stability, as noted by [1]. Figure 10 illustrates the mean EMG envelopes for biceps and triceps during the normalized cycle. The capacity estimators' values also differed, particularly at low elbow angles: this deviation was reflected in the biceps EMG envelopes. A low threshold has been set to highlight the effects of control, but it could be personalized depending on the endurance/fatigue of each individual or based on ergonomic criteria. The EMG data indicated increased triceps activation in the assistance with TAC, with this effect being more pronounced at low elbow angles. This may be explained by the fact that the torque estimator tended to over-assist the task by pushing the forearm upwards when it underestimated the effort-generating capacity for flexion. This imbalance shifted the workload between the flexor and extensor muscles, requiring the extensors to compensate by pulling the forearm down. The MSC therefore has a more robust behavior outside the model calibration range, and therefore a wider validity range.

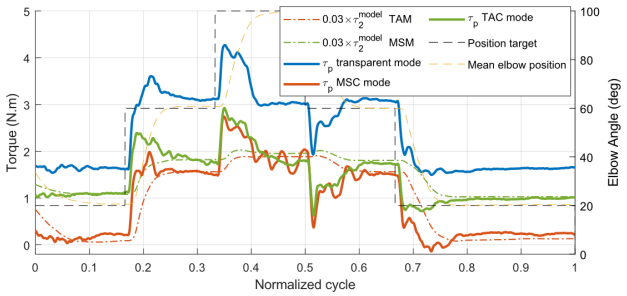


Fig. 9. Limit torques ($0.03\times\tau_2^{model}$) averaged over all participants for TAM and MSM estimators. $\tau_p$ is averaged over all participants for transparent, TAC and MSC modes as a function of the normalized cycle.

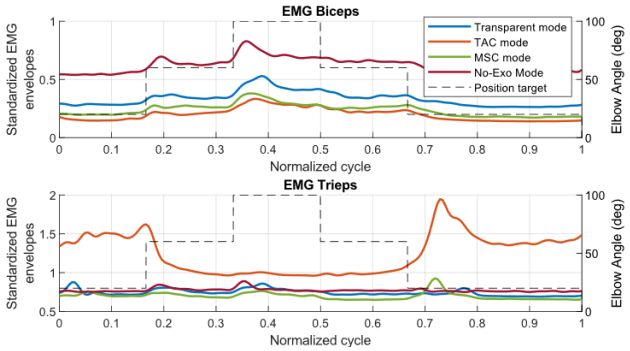


Fig. 10. EMG envelope averages for biceps (top) and triceps (bottom) and for each of the transparent, TAC, MSC and No-Exo modes.

In the transparent configuration, the EMG envelopes for the biceps and triceps were lower compared to the No-Exo configuration, despite the fact that the transparent mode was not assisting the user. Figure 11 illustrates the EMG envelopes for the shoulder deltoids. A similar reduction was observed for the anterior (DA) and medial (DM) deltoids. In contrast, the posterior deltoid (PD) was more active with the exoskeleton. This can be explained by two factors: 1) the exoskeleton passive structure supported the shoulder,thus altering muscle stabilization, and 2) joint angle reconstruction showed differing shoulder positions between conditions (Figure 12), thus affecting muscle force capacity and complicating EMG comparisons. The reduction in EMG envelopes between transparent and assisted modes is therefore a more accurate representation of the assistance provided.

Other limitations may be considered in this work. First, this study focused solely on static estimation. Effort generation capabilities are known to change dynamically during motion [11], and it raised issues in the admittance control during movement phases. A more accurate detection of intention therefore is then necessary. Secondly, the comparison between the joint model and the MSM was restricted to a single joint. As noted by [5], [6], the elbow torque capacity is significantly influenced by the shoulder position. However, linking joints within an articular model

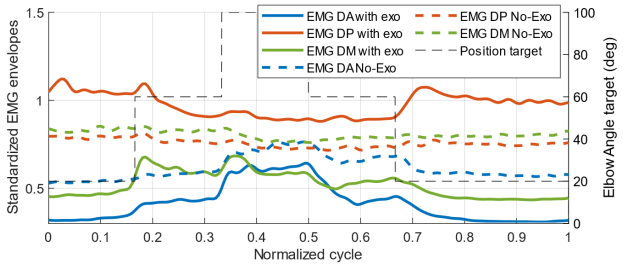


Fig. 11. EMG envelope averages normalized for Deltoid Anterieur (DA), Deltoid Medial (DM) and Deltoid Posterieur (DP) with the exoskeleton and whitout (No-Exo mode).

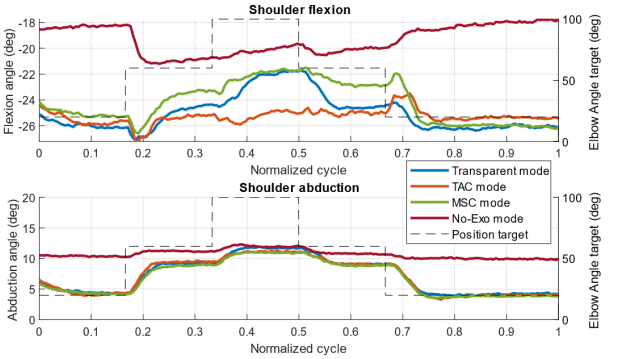


Fig. 12. Averaged shoulder flexion (top) and extension (bottom) for all participants and for each of the transparent, TAC, MSC and No-Exo modes.

with a reasonable number of measurements is challenging. Consequently, MSMs may perform better when multiple joints are considered simultaneously. Lastly, we assumed a known object mass throughout the study. In real-world applications, estimating the mass of the object directly from the exoskeleton measurement will be essential.

## IV. CONCLUSION

Incorporating an effort-generating capacity estimator into shared control systems allows for assistance tailored to the user's needs. Here, we compared two estimators: torque-angle joint model and musculoskeletal model. Both estimators were designed using an assistance control and evaluated with nine participants. The results showed similar performance when movements rely within the calibration range. However, outside this range, the torque-angle joint model proved less robust results than the musculoskeletal model, leading to unintended demands on antagonistic muscles. This preliminary study highlights the limitations of the torque-angle model and highlights the advantages of adopting more sophisticated approaches, such as musculoskeletal modeling.

## V. ACKNOWLEDGMENT

This work was supported by the Inria as part of the Exploratory Action MusMaps and the CONTINUUM project.

## REFERENCES

[1] A. Q. Keemink, H. Van der Kooij, and A. H. Stienen, "Admittance control for physical human–robot interaction," *The International Journal of Robotics Research*, vol. 37, no. 11, pp. 1421–1444, 2018.

[2] T. Proietti, N. Jarrassé, A. Roby-Brami, and G. Morel, "Adaptive control of a robotic exoskeleton for neurorehabilitation," in *2015 7th International IEEE/EMBS Conference on Neural Engineering (NER)*. IEEE, 2015, pp. 803–806.

[3] L. Rose, M. C. Bazzocchi, and G. Nejat, "A model-free deep reinforcement learning approach for control of exoskeleton gait patterns," *Robotica*, vol. 40, no. 7, pp. 2189–2214, 2022.

[4] M. G. Carmichael and D. Liu, "Estimating physical assistance need using a musculoskeletal model," *IEEE Transactions on Biomedical Engineering*, vol. 60, no. 7, pp. 1912–1919, 2013.

[5] L. A. Frey-Law, A. Laake, K. G. Avin, J. Heitsman, T. Marler, and K. Abdel-Malek, "Knee and elbow 3d strength surfaces: peak torque-angle-velocity relationships," *Journal of applied biomechanics*, vol. 28, no. 6, pp. 726–737, 2012.

[6] D. Haering, C. Pontonnier, N. Bideau, G. Nicolas, and G. Dumont, "Using torque-angle and torque–velocity models to characterize elbow mechanical function: Modeling and applied aspects," *Journal of Biomechanical Engineering*, vol. 141, no. 8, p. 084501, 2019.

[7] A. Muller, D. Haering, C. Pontonnier, and G. Dumont, "Non-invasive techniques for musculoskeletal model calibration," in *Congrès Français de Mécanique*, 2017.

[8] W. Wu, P. V. Lee, A. L. Bryant, M. Galea, and D. C. Ackland, "Subject-specific musculoskeletal modeling in the evaluation of shoulder muscle and joint function," *Journal of biomechanics*, vol. 49, no. 15, pp. 3626–3634, 2016.

[9] A. Skuric, V. Padois, N. Rezzoug, and D. Daney, "On-line feasible wrench polytope evaluation based on human musculoskeletal models: an iterative convex hull method," *IEEE robotics and automation letters*, vol. 7, no. 2, pp. 5206–5213, 2022.

[10] K. R. Saul, X. Hu, C. M. Goehler, M. E. Vidt, M. Daly, A. Velisar, and W. M. Murray, "Benchmarking of dynamic simulation predictions in two software platforms using an upper limb musculoskeletal model," *Computer methods in biomechanics and biomedical engineering*, vol. 18, no. 13, pp. 1445–1458, 2015.

[11] F. E. Zajac, "Muscle and tendon: properties, models, scaling, and application to biomechanics and motor control." *Critical reviews in biomedical engineering*, vol. 17, no. 4, pp. 359–411, 1989.

[12] B. A. Garner and M. G. Pandy, "Estimation of musculotendon properties in the human upper limb," *Annals of biomedical engineering*, vol. 31, pp. 207–220, 2003.

[13] W. van Dijk, H. van der Kooij, B. Koopman, and E. H. van Asseldonk, "Improving the transparency of a rehabilitation robot by exploiting the cyclic behaviour of walking," in *2013 IEEE 13th International Conference on Rehabilitation Robotics (ICORR)*, 2013, pp. 1–8.

[14] D. Verdel, A. Farr, T. Devienne, N. Vignais, B. Berret, and O. Bruneau, "Human movement modifications induced by different levels of transparency of an active upper limb exoskeleton," *Frontiers in Robotics and AI*, vol. 11, p. 1308958, 2024.

[15] J. Steven Moore and A. Garg, "The strain index: a proposed method to analyze jobs for risk of distal upper extremity disorders," *American Industrial Hygiene Association Journal*, vol. 56, no. 5, pp. 443–458, 1995.

[16] G. Wu, F. C. Van der Helm, H. D. Veeger, M. Makhsous, P. Van Roy, C. Anglin, J. Nagels, A. R. Karduna, K. McQuade, X. Wang *et al.*, "Isb recommendation on definitions of joint coordinate systems of various joints for the reporting of human joint motion—part ii: shoulder, elbow, wrist and hand," *Journal of biomechanics*, vol. 38, no. 5, pp. 981–992, 2005.

[17] M. Manzano, S. Guégan, R. Le Breton, L. Devigne, and M. Babel, "Force-triggered control design for user intent-driven assistive upper-limb robots," in *IEEE/RSJ Int. Conf. on Intelligent Robots and Systems, IROS'24*, 2024.

[18] H. J. Hermens, B. Freriks, R. Merletti, D. Stegeman, J. Blok, G. Rau, C. Disselhorst-Klug, and G. Hägg, "European recommendations for surface electromyography," *Roessingh research and development*, vol. 8, no. 2, pp. 13–54, 1999.

[19] P. Konrad, "The abc of emg," *A practical introduction to kinesiological electromyography*, vol. 1, no. 2005, pp. 30–5, 2005.

[20] S. L. Delp, F. C. Anderson, A. S. Arnold, P. Loan, A. Habib, C. T. John, E. Guendelman, and D. G. Thelen, "Opensim: open-source software to create and analyze dynamic simulations of movement," *IEEE transactions on biomedical engineering*, vol. 54, no. 11, pp. 1940–1950, 2007.

[21] A. Seth, R. Matias, A. P. Veloso, and S. L. Delp, "A biomechanical model of the scapulothoracic joint to accurately capture scapular kinematics during shoulder movements," *PloS one*, vol. 11, no. 1, p. e0141028, 2016.